Rheology, Morphology, and Crystallization Behavior of Melt-Mixed Blends of Polyamide6 and Acrylonitrile-Butadiene-Styrene: Influence of Reactive Compatibilizer Premixed with Multiwall Carbon Nanotubes

Suryasarathi Bose,[1] Arup R. Bhattacharyya,[1] Pravin V. Kodgire,[2] Ashok Misra,[2] Petra Pötschke[3]

[1]*Department of Metallurgical Engineering and Materials Science, Indian Institute of Technology Bombay, Powai, Mumbai 400076, India*
[2]*Department of Chemical Engineering, Indian Institute of Technology Bombay, Powai, Mumbai 400076, India*
[3]*Department of Polymer Reactions and Blends, Leibniz Institute of Polymer Research Dresden, Hohe Strasse 6, D-01069 Dresden, Germany*

Received 20 April 2007; accepted 25 June 2007
DOI 10.1002/app.27018
Published online 21 August 2007 in Wiley InterScience (www.interscience.wiley.com).

ABSTRACT: Blends of polyamide6 (PA6) and acrylonitrile butadiene styrene (ABS) were prepared in presence or absence of up to 5 wt % of a reactive compatibilizer [styrene maleic anhydride copolymer (SMA) modified with 5 wt % multiwall carbon nanotubes (MWNT)] by melt-mixing using conical twin screw microcompounder where the ABS content was varied from 20 to 50 wt %. The melt viscosity of the blends was significantly enhanced in presence of SMA modified by multiwall carbon nanotubes due to the reactive compatibilization, which leads to stabilized interphase in the blends. Furthermore, the presence of MWNT in the compatibilizer phase led to additional increase in viscosity and storage modulus. Morphological studies revealed the presence of either droplet-dispersed or cocontinuous type depending on the blend compositions. Further, reactive compatibilization led to a significant change in the morphology, namely a structure refining, which was enhanced by MWNT presence as observed from SEM micrographs. DSC crystallization studies indicated a delayed crystallization response of PA6 in presence of ABS presumably due to high melt viscosity of ABS. The crystallization temperature and the degree of crystallinity were strongly dependent on the type of morphology and content of reactive compatibilizer, whereas the presence of MWNT had an additional influence. SAXS studies revealed the formation of thinner and less perfect crystallites of PA6 phase in the blends, which showed cocontinuous morphology. A unique observation of multiple scattering maxima at higher q region has been found in the blends of cocontinuous morphology, which was observed to be successively broadened in presence of the compatibilizer. J Appl Polym Sci 106: 3394–3408, 2007

Key words: compatibilization; crystallization; morphology; MWNT; PA6/ABS blends

INTRODUCTION

Blending of polymers is an important tool that often gives rise to the possibility of enhancing the overall properties of the material through a synergistic combination of desirable properties from each component. However, most polymer blends are immiscible because of their high molecular weight and unfavorable interactions, thus forming multiphase structures. Morphology is a key parameter next to the properties of component polymers in determining the properties of multiphase polymeric materials.[1,2]

Two major types of morphology can be observed for melt blended immiscible polymers: the matrix dispersed droplet structure and the cocontinuous structure. In cocontinuous blends, both components form phases that partly or fully form a continuous phase. The thermodynamically unstable cocontinuous morphology is often observed for blends of a composition near phase inversion. Such morphologies can be stabilized by the use of a compatibilizer, which resides at the polymer/polymer interface and reduces the interfacial tension between the blend components and prevents coalescence via steric stabilization.[3–7] However, the final morphology generated during the melt processing of the blends critically depends on the composition, viscosity, and elasticity ratio and interfacial tension between the components. It is believed that ''emulsion effect'' and ''interlayer slip'' are the two mechanisms operating the melt viscosity in immiscible polymer blends.[8] It is also observed that the existence of

Correspondence to: A. R. Bhattacharyya (arupranjan@iitb.ac.in).

Contract grant sponsor: Department of Science and Technology (DST), India (SERC Fast Track Scheme); contract grant number: 04DS047.

cocontinuous structure is manifested in significant increase in viscosity particularly at low frequencies.[9] Further, reactive compatibilization also results in increase in the melt viscosity manifesting the interfacial activity at the blends interface by the compatibilizer.[8]

Next to morphology, the crystallization behavior of semicrystalline component in immiscible polymer blends has received much attention. The crystallization behavior of the matrix being affected in presence of the second component for uncompatibilized and compatibilized polymer blends is widely reported in the literature.[10–13]

It has been shown that blending of polyamide6 (PA6) with other polymers may induce drastic changes in the crystallization behavior of the continuous PA6 phase.[14–19] For example, addition of EPDM in PA6/EPDM blends decreases the overall crystallinity of the PA6 phase with increasing EPDM content.[14] Similar results were observed by Martuscelli et al.[15] in PA6/rubber blends. The crystallization behavior of one component being affected by the presence of the other phase was successfully demonstrated by Bhattacharyya et al.[16] in PA6/EVA blends system and by Beltrame et al.[17] in PA6/PP blends system. The morphology induced changes in the crystallization behavior of binary blends was well corelated by Jafari et al.[18] in the multicomponent blend system based on PA6, styrene-acrylonitrile copolymer (SAN), and acrylonitrile butadiene styrene (ABS), where the second component had a nucleating effect and improved the overall degree and rate of crystallization of PA6. Further, the delay in the crystallization behavior in the PA6 phase was observed by Araújo et al.[19] when the morphology changed from matrix-droplet to cocontinuous type in the PA6/ABS blend system. Hage et al.[20] has also shown similar behavior for PBT/ABS binary blends where ABS has significantly reduced the crystallization temperature and the heat of crystallization of PBT matrix phase.

ABS is a well-known thermoplastic polymer, which consists of butadiene rubber dispersed in a matrix of SAN. The use of ABS to modify some of the properties of PA6 was reported in the past.[21–29] The concept of reactive compatibilization and the use of styrene-maleic anhydride copolymer (SMA) as an effective compatibilizer for PA6/ABS system was described extensively.[29–32]

Recently carbon nanotubes have emerged as a potential candidate as filler in polymer based composites because of their unique mechanical, electrical, and thermal properties.[33] The addition of carbon nanotubes significantly affecting the crystallization behavior of semi-crystalline polymer has recently been explored.[34–38] Addition of carbon nanotubes altering the melt rheological behavior of polycarbonate and its blend with polyethylene was well established by Pötschke et al.[39,40]

In our previous paper we studied the effect of SMA modified by multiwall carbon nanotubes (MWNT) on the fractionated crystallization behavior of PA6 in PA6/ABS blends, where PA6 was in the minor phase.[41] In this work premixed SMA copolymer modified by MWNT is utilized as a reactive compatibilizer. It is one of the expectations that SMA would reside at the interface of the PA6/ABS blends. Since MWNT are well dispersed in SMA matrix in the premixed SMA/MWNT composites, one can expect that MWNT would also locate at the interface, which will subsequently alter the rheology of the interface and stabilize the morphology by inhibiting coalescence. Thus, it motivated us to study the rheology, morphology, and crystallization behavior of PA6/ABS blends where PA6 forms a continuous phase either as a matrix in 80/20 PA6/ABS blends or in cocontinuous 50/50 blends in presence of a reactive compatibilizer modified by MWNT (SMA modified by MWNT).

EXPERIMENTAL

Materials and specimen preparation

Polyamide6 (PA6) with a zero shear viscosity of 180 Pa s at 260°C was obtained from GFSC, Gujarat, India (Gujlon M28RC, relative viscosity 2.8, M_v is 38,642 in 85% formic acid). Acrylonitrile-butadiene-styrene (ABS) copolymer (Absolac-120, with typical composition consisting of acrylonitrile: 24 wt %, rubber content: 16.5 wt % and styrene: 59.5 wt %) was supplied by Bayer ABS Ltd., India. Multiwall carbon nanotubes (MWNT) were obtained from Iljin Nanotech, Korea, which were synthesized by CVD technique of purity level >90% (Length = 10–50 μm, Diameter = 10– 20 nm). The PA6/ABS blends were prepared by melt mixing in a conical twin-screw extruder (Micro 5, DSM Research, Netherlands) at 260°C with a rotational speed of 150 rpm for 5 min where ABS content was varied from 20 to 50 wt %. Preblended styrene maleic anhydride (SMA) and MWNT of 95 : 5 ratio (wt/wt) (here after assigned as SMA modified by MWNT denoted by ''M'') was used as a compatibilizer and prepared by melt-mixing under the same extrusion conditions. The detailed blend compositions with their sample codes are listed in Tables Ia and Ib. The DSM microcompounder with a capacity of 5 cc has two conical corotating screws with a bypass allowing the material to circulate for defined periods. After the desired mixing time, the mixture was taken out through the die by opening the valve. Prior to mixing the materials were dried for 24 h at 80°C in a vacuum oven. Compression moulded films with 0.5-mm thickness were prepared at 260°C.

TABLE Ia
Sample Code, Compositions, and Continuity of ABS Phase in PA6/ABS Blends

Sample code	PA6 (wt %)	ABS (wt %)	Continuity of ABS phase (%)
PA6	100	–	–
ABS	–	100	–
N80A20	80	20	17.3
N65A35	65	35	90.8
N60A40	60	40	91.0
N55A45	55	45	98.3
N50A50	50	50	98.8

Characterization

The rheological measurements were performed using an ARES oscillatory rheometer (Rheometric Scientific, USA) at 260°C under nitrogen atmosphere with parallel plate geometry (plate diameter of 25 mm, gap of 1–2 mm). Frequency sweeps were carried out between 0.1 and 100 rad/s. The strains used were chosen in order to be within the linear viscoelastic range.

Scanning electron microscopy (SEM) was performed using FEI Quanta 200 and Hitachi S3400 with gold sputtering on the etched surface. The extruded strands were cryo-fractured using liquid nitrogen and etched with formic acid for 24 h at room temperature to remove the PA6 phase of the blends. Cryofractured strands were also etched with boiling tetrahydrofuran (THF) for 45 min to remove the ABS phase of the blends.

The continuity of the ABS phase (%) in PA6/ABS blends was determined by selective extraction technique. For the blend system used, ABS can be extracted using THF, which does not dissolve, swell, or penetrate the PA6 phase. Extruded strands of 2 cm length were kept in THF at room temperature for 4 days, to remove the ABS phase from the blends. Samples were washed with fresh solvent after 24 h and were kept in the fresh solvent. At the end of the 4th day samples were removed and dried in the vacuum oven. The continuity of the ABS phase (%) was made by taking the ratio of weight difference before and after the selective extraction process and the initial weight of the ABS portion in the blends.

TABLE Ib
Sample Code and Compositions of PA6/ABS Blends with or without SMA-Modified MWNT

Sample code	PA6 (wt %)	ABS (wt %)	SMA (wt %)	MWNT (wt %)
N50A50S2	49	49	2	–
N50A50M1	49.5	49.5	0.95	0.05
N50A50M2	49	49	1.9	0.1
N50A50M5	47.5	47.5	4.75	0.25
N80A20S2	78.4	19.6	2	–
N80A20M1	79.2	19.8	0.95	0.05
N80A20M2	78.4	19.6	1.9	0.1
N80A20M5	76	19	4.75	0.25

TABLE Ic
Morphological Parameters of 80/20 PA6/ABS Blends with or without SMA-Modified MWNT

Sample code	D_n (μm)	D_w (μm)
N80A20	1.67	2.12
N80A20S2	0.74	1.35
N80A20M1	1.20	1.50
N80A20M2	0.64	0.96
N80A20M5	0.4	0.42

Three micrographs of different magnifications showing in average 200 etched holes were considered to evaluate the number average diameter (D_n) and weight average diameter (D_w) of ABS in 80/20 PA6/ABS blends with or without SMA modified by MWNT. The number–average diameter (D_n) and the weight–average diameter (D_w) of the ABS droplets were calculated using the following equations:

$$D_n = \left(\sum n_i d_i\right)/\left(\sum n_i\right)$$

$$D_w = \left(\sum n_i d_i^2\right)/\left(\sum n_i d_i\right)$$

where, n_i indicates the number of droplets having d_i as their diameter.

Differential scanning calorimetric (DSC) measurements were carried out using Perkin Elmer DSC-6 using Pyris software. The extruded samples of about

TABLE II
DSC Melting and Crystallization Parameters for PA6 and Blends of PA6/ABS and for Blends of 50/50 PA6/ABS and 80/20 PA6/ABS with or without SMA-modified MWNT

Sample code	T_m (°C)	T_c (°C)	$(\Delta H_c)_{norm}$ (J/g)
For PA6 and blends of PA6/ABS			
PA6	(216.9, 220.9)	192.8	69.0
N80A20	(214.8, 220.1)	192.1	82.0
N65A35	(213.8, 220)	191.2	70.5
N60A40	(214, 220)	190.3	68.0
N55A45	(214.3, 220)	190.8	64.0
N50A50	(215.8, 221.1)	191.1	56.4
Blends of 50/50 PA6/ABS			
N50A50	(215.8, 221.1)	191.1	56.4
N50A50S2	(215, 221)	190.7	75.5
N50A50M1	217	193.0	64.6
N50A50M2	217	192.2	64.2
N50A50M5	217	192.0	63.2
Blends of 80/20 PA6/ABS			
N80A20	(214.8, 220.1)	192.1	82.0
N80A20S2	(215, 220)	190.6	81.0
N80A20M1	(216, 220)	193.0	72.2
N80A20M2	216	192.3	75.2
N80A20M5	216	191.4	77.7

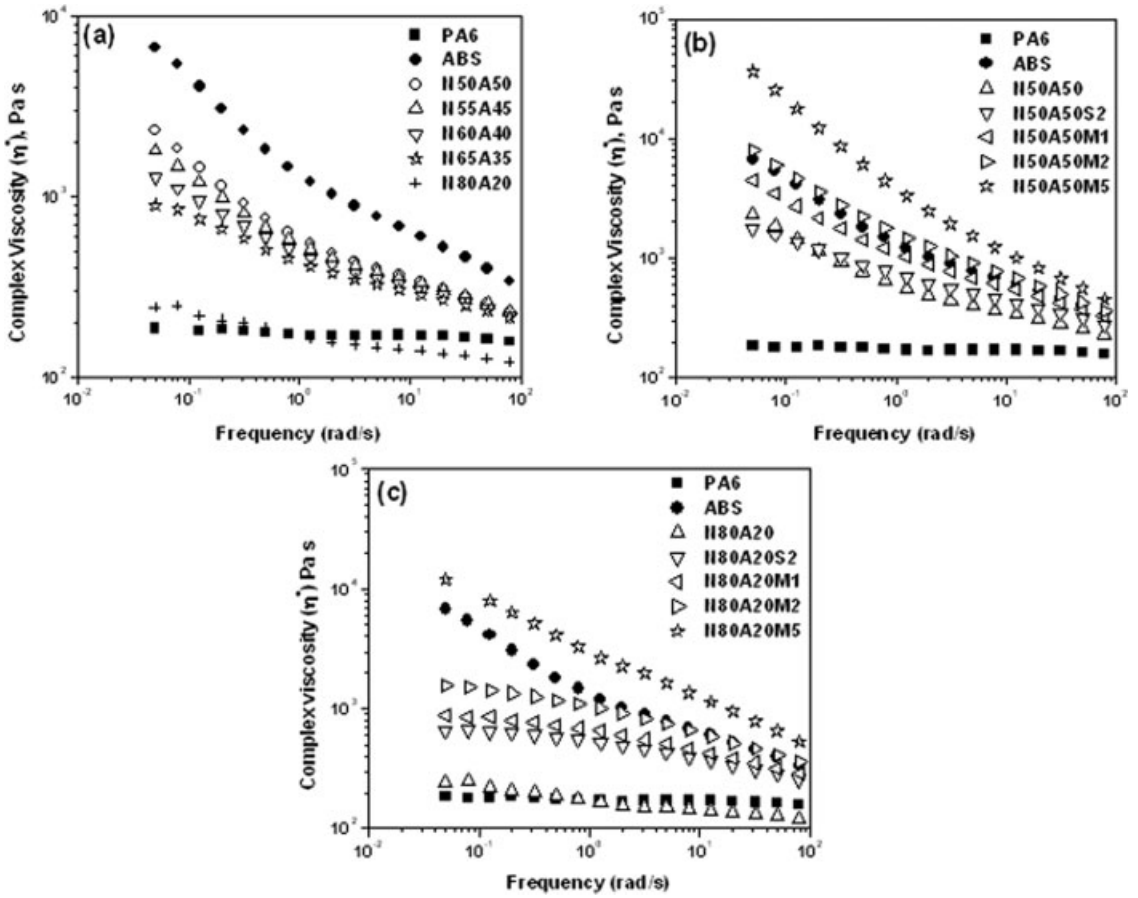

Figure 1 Complex viscosity versus frequency plots of (a) neat PA6/ABS blends; (b) 50/50 PA6/ABS blends with or without SMA modified by MWNT; (c) 80/20 PA6/ABS blends with or without SMA modified by MWNT.

5 mg were dried in a vacuum oven prior to experiment. The heating-cooling-heating cycles were recorded in the temperature range from 10 to 260°C at a scan rate of ±10 K/min under nitrogen atmosphere. Temperature and transition heat were calibrated with indium standard. In the first heating run all samples were annealed at the final temperature (260°C) for 3 min to delete the previous thermal history. The heat of fusion (ΔH_m) of PA6 phase was normalized to the fraction of PA6 present in the blends. The heat of crystallization (ΔH_c) was also normalized to the fraction of PA6 in the blends [the heat of fusion of 100% crystalline PA6, $(\Delta H_m)_0$ was taken as 204.8 J/g[42]].

Wide-angle X-ray diffraction (WAXD) studies were carried out on a Philips X-Pert Pro. The incident X-rays (λ = 1.54 Å) from the Cu-target were monochromatized using a Ni filter. Compression moulded samples of 0.5-mm thickness were used as test specimens. WAXD patterns were recorded with a step scan with step size of 0.02 between 5° and 40° 2θ.

Small angle X-ray scattering (SAXS) experiments were performed with line collimation geometry, using SAXSess camera (Anton Paar). The Cu-K_α incident radiation from PANalytical X-ray source at 40 kV (40 mA) was used. Samples were kept in between the copper plates for 15 min. Image plate reader (Packard Bioscience) was used to record the scattering and the images were generated by software: OptiQuant (Packard Bioscience). The SAXSquant produces one-dimensional scattering curves by averaging two-dimensional scattering patterns over linear or circular paths.

RESULTS AND DISCUSSIONS

Rheological behavior of PA6/ABS blends

The melt rheological response during frequency sweep for polyamide6 (PA6)/acrylonitrile butadiene styrene (ABS) blends along with pure PA6 and ABS is shown in Figure 1 (complex viscosity versus frequency) and Figure 2 (storage modulus versus frequency). Pure PA6 shows Newtonian flow behavior in the measured frequency range as complex viscosity is found to be independent of the frequency [Fig. 1(a)]. Further, the melt viscosity of the ABS phase is found to be much higher as compared with the PA6 phase in the measured range of frequency. However,

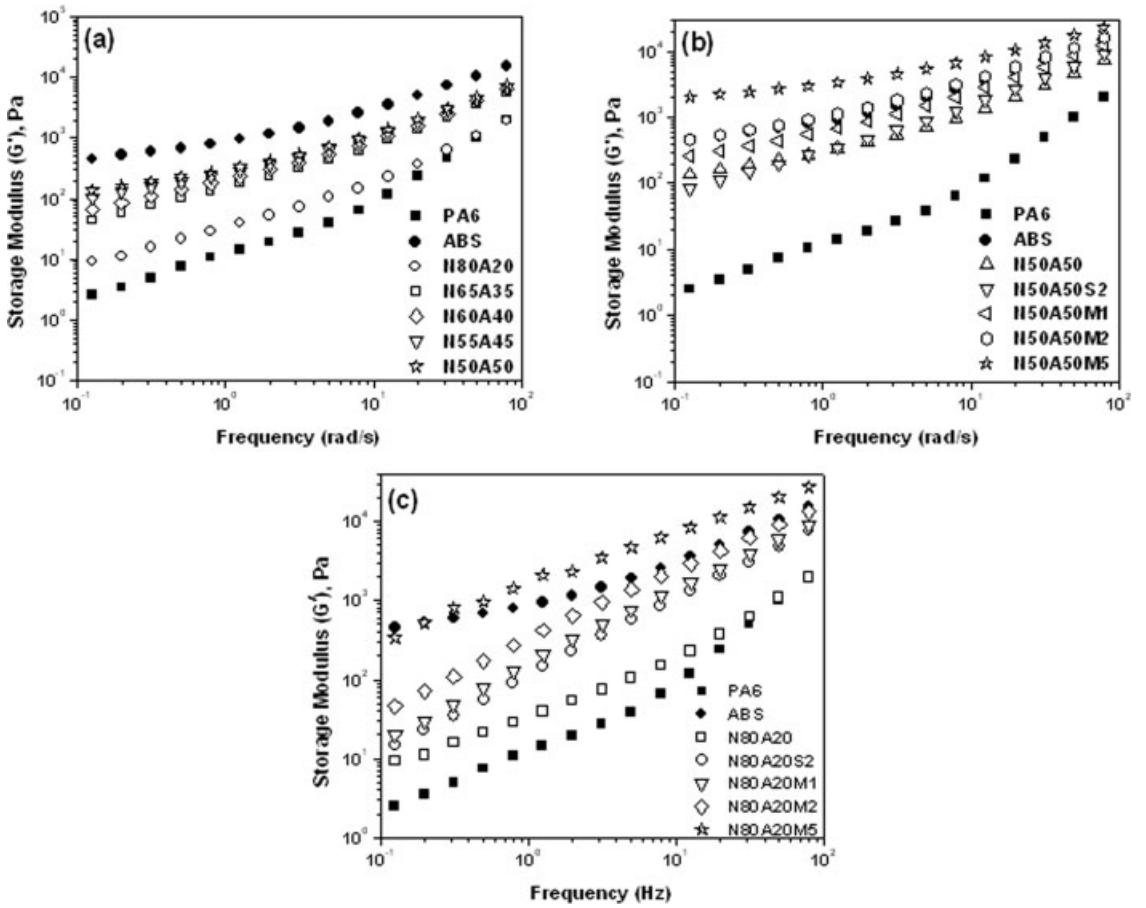

Figure 2 Storage modulus versus frequency plots of (a) neat PA6/ABS blends; (b) 50/50 PA6/ABS blends with or without SMA modified by MWNT; (c) 80/20 PA6/ABS blends with or without SMA modified by MWNT.

ABS shows a linear decrease in melt viscosity with increase in frequency, indicating the existence of a yield stress. Figure 1(a) also indicates that the melt viscosity of the PA6/ABS blends follow a simple mixing rule (except for 80/20 composition), melt viscosity is found to increase with ABS content at each frequency. The existence of yield stress at low frequency is also evident in PA6/ABS blends. Figure 1(b) compares the complex viscosity of the 50/50 PA6/ABS blends with or without styrene maleic anhydride (SMA) modified by MWNT. The observed increase in melt viscosity is presumably due to combined effect of reactive compatibilization and changes in the rheological behavior of the interphase by addition of MWNT. On addition of 2 and 5 wt % premixed SMA modified by MWNT to 50/50 PA6/ABS blends we observed a positive deviation in the melt viscosity manifesting in higher melt viscosity even than neat ABS. To get more insight into the fact whether the efficiency of the reactive compatibilizer is morphology dependent we studied the rheological behavior of 80/20 PA6/ABS blends in presence or absence of SMA modified by MWNT. On comparing the melt viscosity of 80/20 PA6/ABS blends [Fig. 1(c)] with or without SMA modified by MWNT we found a plateau in the lower frequency region up to 2 wt % premixed SMA modified by MWNT. In case of 5 wt % premixed SMA modified MWNT the melt viscosity shows a linear decrease with increasing frequency and is even found to be higher than ABS. To investigate further the individual role of SMA and MWNT affecting the rheological behavior of the blends we compared the melt viscosity of 2 wt % premixed SMA modified by MWNT and 2 wt % SMA blended with PA6/ABS blends. Interestingly, the melt viscosity is found to be higher in case of 2 wt % premixed SMA modified by MWNT as compared to only 2 wt % SMA blended with PA6/ABS blends in case of both 50/50 [Fig. 1(b)] and 80/20 PA6/ABS blends [Fig. 1(c)]. This observation clearly manifests the role of MWNT at the blend interphase affecting the melt viscosity of SMA modified by MWNT in PA6/ABS blends.

Figure 2(a) depicts an increase of storage modulus with increase in frequency for pure PA6, whereas the development of a plateau in storage modulus is observed at low frequency range in case of ABS. A similar behavior is observed in the storage modulus

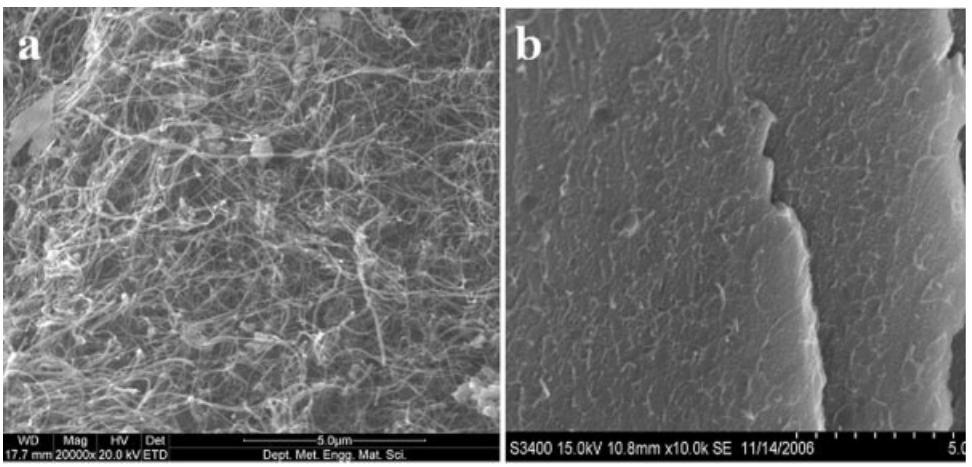

Figure 3 (a) SEM of MWNT; (b) SEM of SMA modified by MWNT (95/5, wt %/wt %).

versus frequency curves for PA6/ABS blends, which follow a linear mixing rule. In case of 50/50 blends with SMA modified by MWNT, the storage modulus of premixed 2 wt % SMA modified by MWNT is comparable with neat ABS and the storage modulus of premixed 5 wt % SMA modified by MWNT is even higher than neat ABS [Fig. 2(b)]. This is presumably due to a reinforcing effect of the interface by the presence of MWNT. In this context it is worthy to mention that use of reactive compatibilizer in an immiscible blend system often leads to higher interfacial area and higher entanglement at the interface leading to improved storage modulus. In our case the interface is modified due to increased interfacial area in presence of a reactive compatibilizer (SMA) and since MWNT are also located at the interface the combined effect results in higher storage modulus values in blends. A similar behavior is also observed in case of 80/20 blends [Fig. 2(c)]. Further, storage modulus of 2 wt % premixed SMA modified by MWNT is found to be higher as compared to 2 wt % SMA blended with PA6/ABS blends in both 50/50 and 80/20 compositions indicating the pronounced effect of MWNT at the blends interphase.

Morphological analysis

Figure 3(a) shows a SEM micrograph of the MWNT used in this work. The existence of highly entangled network-like structure of MWNT is well evident from the micrograph. A percolated MWNT network structure and relatively good dispersion of MWNT are evident in SMA/MWNT composites [95/5, wt %/wt %, Fig. 3(b)], which is used as the reactive compatibilizer in the PA6/ABS blends. Figure 4 shows the SEM micrographs of cryofractured surfaces etched in THF (to remove ABS) of PA6/ABS blend wherein ABS content is varied from 20 to 50 wt %. Figure 4(a) illustrates that the 80/20 PA6/ABS blend exhibits matrix-dispersed droplet type morphology in which the ABS phase is dispersed as spherical droplets. The blend morphology remains as matrix-dispersed droplet type at 35 wt % ABS level [Fig. 4(b)]. Figure 4(c–e) of the SEM micrographs indicates that the phase morphology is predominantly of cocontinuous type when ABS content is varied towards 40 and 50 wt %. The cocontinuous morphology at these compositions [Fig. 4(c,e)] also reveals some spherical inclusion of ABS phase in the continuous PA6 phase. The continuity of ABS phase was calculated by taking the ratio of the ABS phase before and after selective extraction in THF from the respective blend compositions, which is shown in Table Ia. The continuity values of the ABS phase (%) further indicate that 80/20 PA6/ABS blends exhibit a matrix-dispersed droplet type morphology, whereas, PA6/ABS blends containing 35–50 wt % ABS showed cocontinuous morphology as %continuity of ABS phase is >90% upto 40 wt % ABS content and >98% in case of 45 and 50 wt % ABS content. Cocontinuous morphology (Fig. 5) of 65/35 PA6/ABS and 50/50 PA6/ABS blends was reconfirmed by performing the SEM analysis of the respective blend compositions where the PA6 phase was etched by formic acid.

Figure 6(a–e) shows the SEM micrographs of cryofractured and selectively etched (in THF) surfaces of 50/50 PA6/ABS blends with or without SMA modified by MWNT. Figure 6(b) illustrates the SEM micrograph of 50/50 PA6/ABS blends with 2 wt % SMA. A coarse cocontinuous morphology is observed for this composition, which is presumably due to the fact that the concentration of the compatibilizer is insufficient to produce finer morphology. It is one of the expectations that SMA modified by MWNT would reside at the blend interface and act as an efficient compatibilizer. A consistent refine-

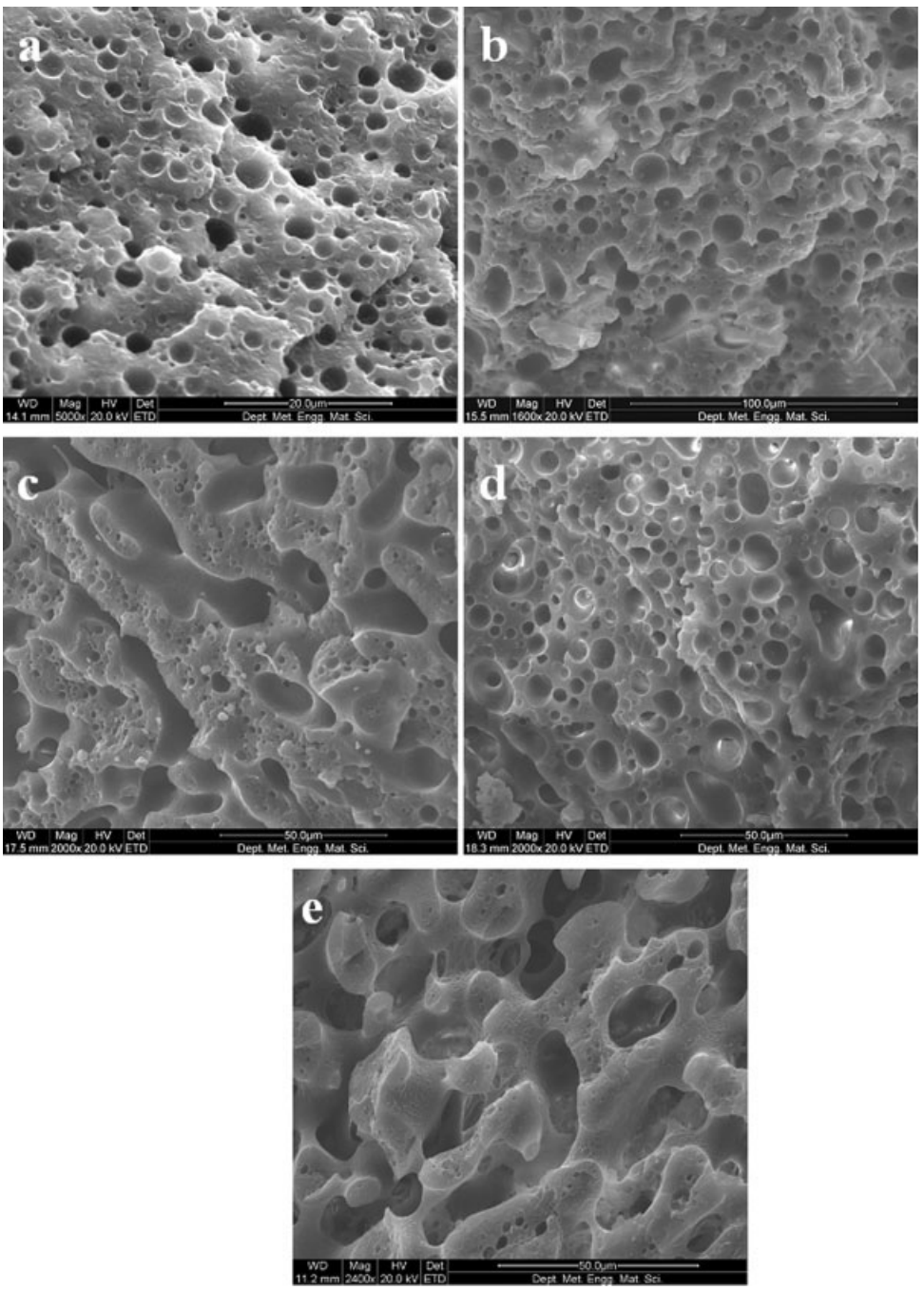

Figure 4 Scanning electron micrographs of cryofractured and selectively etched by THF of blends of PA6/ABS; (a) 80/20, (b) 65/35, (c) 60/40, (d) 55/45, and (e) 50/50.

ment in the cocontinuous morphology is clearly observed in this set of blends with increase in the SMA modified by MWNT [Fig. 6(c–e)] manifesting in finer ligament size of the remaining PA6 phase. Interestingly, the appearance of concave PA6 surfaces in uncompatibilized blend changes to convex PA6 surfaces in presence of SMA modified by MWNT in 50/50 PA6/ABS blends. The structural changes appearing at this composition can be attributed to states just before and above the phase inversion composition. However, the observed change in the morphology is due to the compatibilization of the SMA copolymer, where the anhydride functional group of the SMA is expected to react with the amine end groups of PA6.[43] Figure 7 compares the SEM micrographs of 80/20 PA6/ABS blends with or without SMA modified by MWNT. The efficiency of SMA modified by MWNT as a reactive compatibilizer can well be observed from these micrographs manifesting in a drastic reduction in the domain size

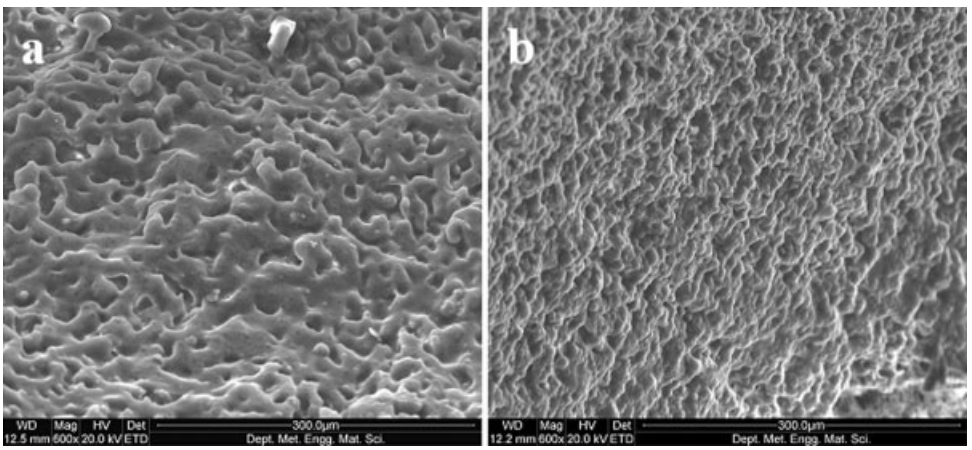

Figure 5 Scanning electron micrographs of cryofractured and selectively etched by formic acid of PA6/ABS blends; (a) 50/50, (b) 65/35 showing cocontinuous morphology.

with increase in the SMA modified by MWNT content. The effectiveness of the compatibilizer is well evident from Table Ic where the drastic reduction in both D_n and D_w can be observed manifesting in submicron size droplets. For 80/20 PA6/ABS blends with 5 wt % premixed SMA modified by MWNT the D_w is about 0.4 μm compared with 2.12 μm for neat 80/20 PA6/ABS blends. Interestingly, on comparing the D_w of 2 wt % premixed SMA modified by MWNT in the 80/20 blends (0.96 μm) and 2 wt % SMA blended with 80/20 PA6/ABS blends (1.35 μm) one can clearly identify the role of MWNT in providing finer domain size distribution in 80/20 PA6/ABS blends. Figure 8(a) shows the high magnification SEM micrographs of 1 wt % premixed SMA modified by MWNT in 50/50 PA6/ABS blends. MWNT are found to bridge between the phases in these micrographs. One can clearly observe that some MWNT are located at the interphase as well as in the PA6 phase. This observation is due to the fact that the length dimensions of the tubes are much larger in size than the phase sizes (ligament sizes) of the blends.[40] A thick layer of SMA copolymer encapsulating the MWNT is also evident from this set of blends, manifested by higher observed diameter of the MWNT. We observed that SMA readily dissolves in THF, whereas the product of melt-interfacial reaction between anhydride functional group of the SMA and the amine end groups of PA6 does not dissolve in THF which is manifested in a thick layer of reactive mass encapsulating the MWNT surface. Figure 8(b) shows the high magnification SEM micrographs of 1 wt % premixed SMA modified by MWNT in 80/20 PA6/ABS blends and confirm the phenomenon of encapsulation in this blend. This encapsulation phenomenon may hinder the heterogeneous nucleation action from the MWNT surface which will be discussed in detail while dealing with the thermal behavior of the blends. We also observed that encapsulation of tubes by the SMA copolymer led to a detrimental effect on the electrical conductivity (not shown here) of the blends.

Melting and crystallization behavior by DSC and WAXD

DSC melting endotherms [Fig. 9(a)] indicate that PA6 and the different blend compositions of PA6/ABS show double melting endotherms during the second heating cycle. The observed double melting endotherms of PA6 is presumably due to polymorphism (presence of both α and γ crystalline forms of PA6), which have been discussed later under the WAXD analysis. It is shown in Table II that the melting temperatures (T_{m1} and T_{m2}) of PA6 remain almost unaffected with increase in ABS in the blends. On the other hand, even if the crystallization temperature (T_c) of PA6 is almost unchanged at 20 wt % ABS content, the heat of crystallization (ΔH_c) of PA6 increased significantly. In addition, with increase in ABS content ΔH_c is found to decrease. Further, T_c is found to decrease marginally with increase in the ABS content in the blend indicating delayed crystallization of PA6 in presence of ABS [Fig. 9(b)], which may be related to the increase in melt viscosity of the blends with increase in ABS phase. A similar observation is also reported for PBT/ABS blends.[20] As SMA is added to the 50/50 PA6/ABS blends, the crystallization temperature (T_c) of PA6 decreases as compared to the neat blends, thereby showing a further delay in the PA6 crystallization process [Fig. 10(a)]. On incorporation of SMA modified by MWNT the crystallization temperature was found to increase moderately indicating the nucleating action of MWNT during the crystallization of the PA6 phase (Table II). Interestingly, further increase in the crystallization temperature is not observed on increasing the MWNT content presum-

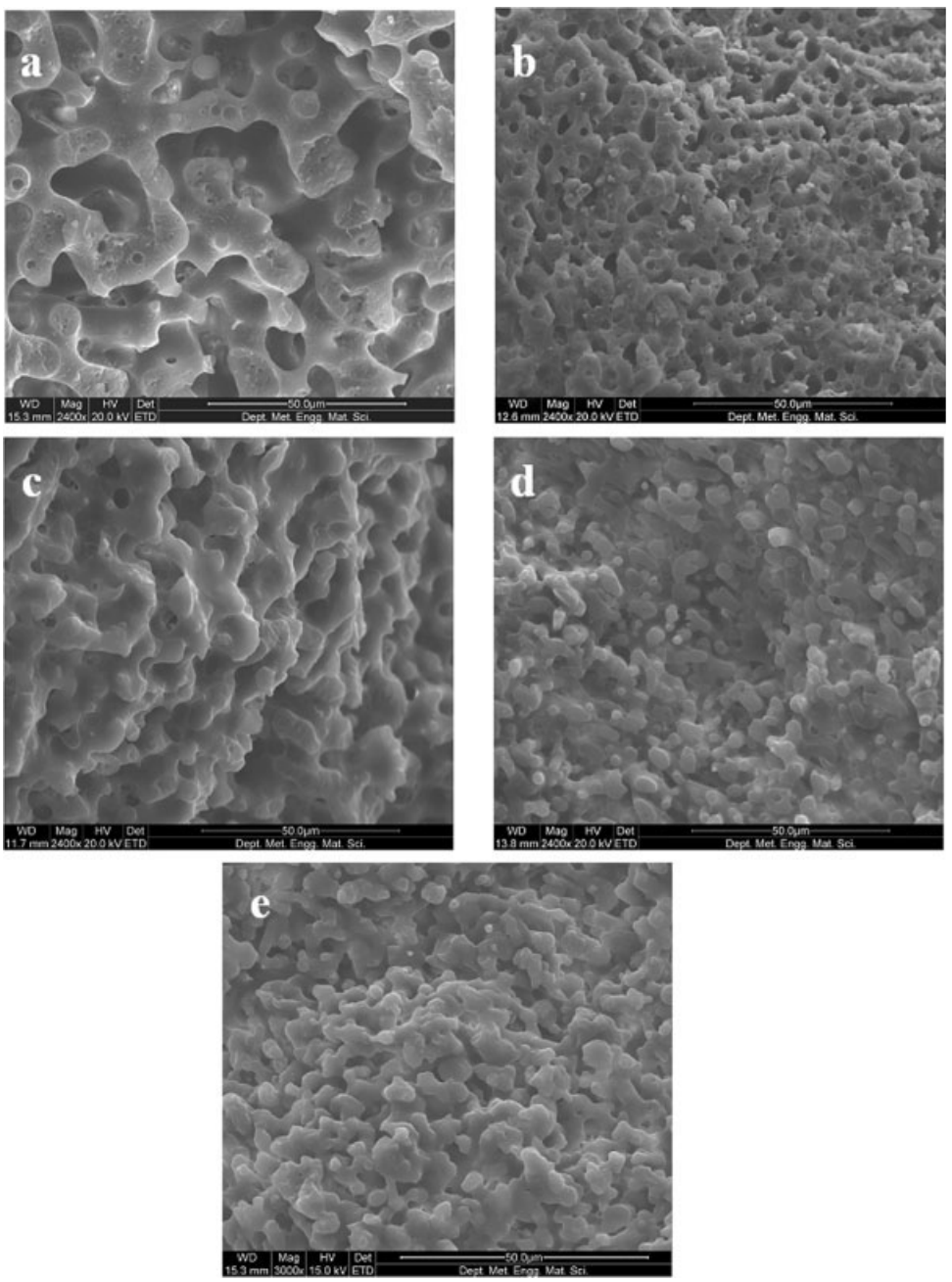

Figure 6 SEM micrographs of cryofractured and selectively etched by THF of; (a) N50A50; (b) N50A50S2; (c) N50A50M1; (d) N50A50M2; and (e) N50A50M5.

ably due to the encapsulation of MWNT by the SMA copolymer. Moreover, as compared with uncompatibilized blends, reactive compatibilized blends show an overall increase in ΔH_c. However, at higher levels of SMA modified by MWNT ΔH_c is found to decrease considerably as compared with neat PA6/ABS blends. The decrease of ΔH_c at higher SMA modified by MWNT level may be related to higher entanglements at the interface, which is presumably hindering the mobility of the crystallizing chain of PA6. In case of 80/20 blends with SMA modified by MWNT even if MWNT is providing heterogeneous nucleating sites, ΔH_c is found to be lower (Table II) as compared with uncompatibilized blends which is presumably due to greater extent of interfacial reaction in presence of SMA modified by MWNT. Further, no significant change in the crystallization temperature is observed due to the encapsulation of MWNT by SMA copolymer [Fig. 10(b)]. Thus, it can be concluded at this stage that ΔH_c and T_c are strongly affected by the increase in the melt viscosity especially if cocontinuous structures are formed in case of uncompatibilized blends, whereas in presence of SMA modified by MWNT in the blends the

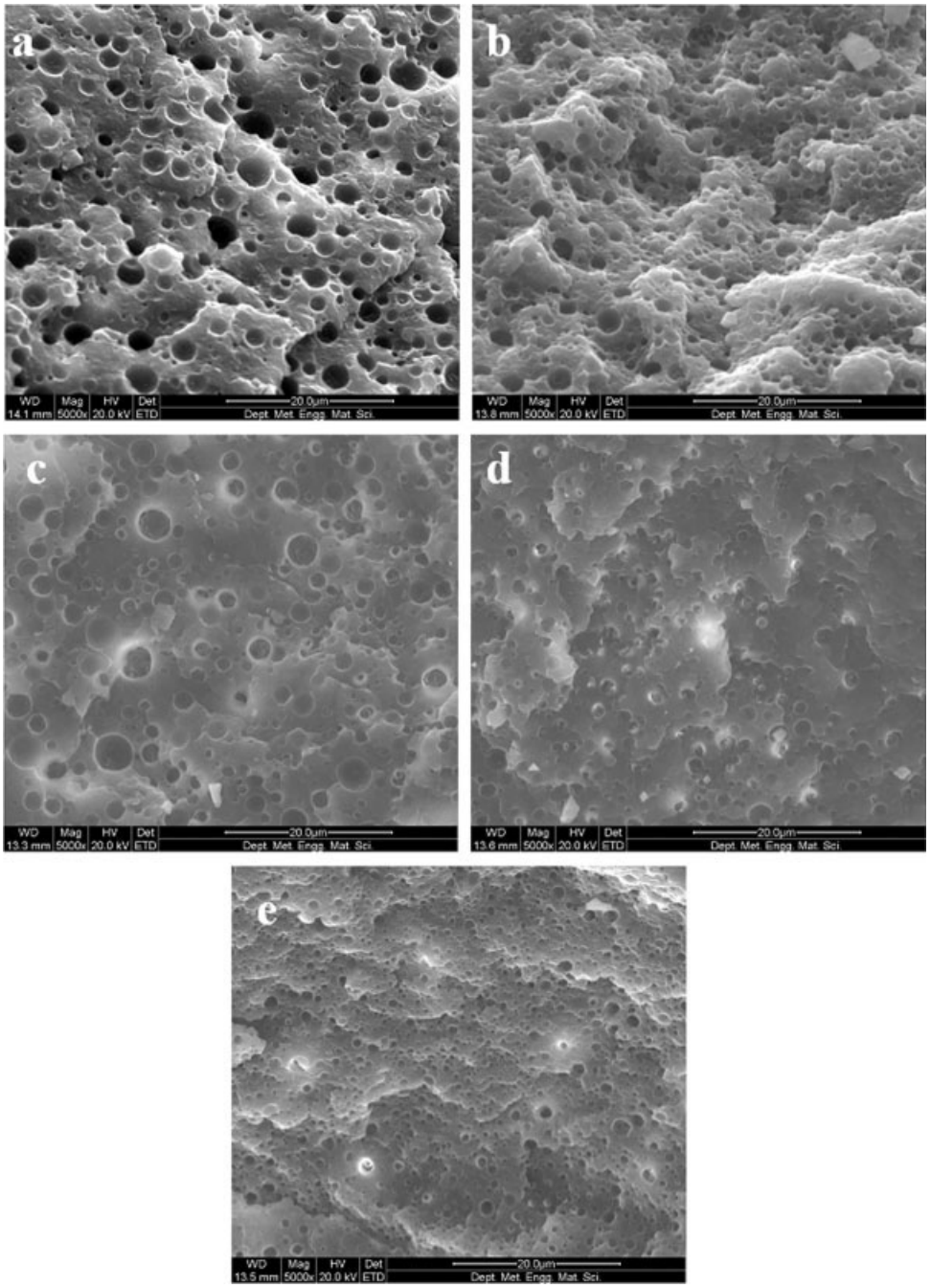

Figure 7 SEM micrographs of cryofractured and selectively etched by THF of (a) N80A20; (b) N80A20S2; (c) N80A20M1; (d) N80A20M2; and (e) N80A20M5.

crystallization behavior of PA6 is affected mainly by two factors. Firstly, by the nucleating action of MWNT and secondly by the increased probability of chain entanglements at the interface due to reactive coupling which perhaps affects the mobility of the crystallizing PA6 chains and which in turn dominates over the melt viscosity factor.

Figure 11 depicts the WAXD pattern for neat PA6/ABS blends, 50/50 and 80/20 PA6/ABS blends with or without SMA modified by MWNT. Two sharp diffraction maxima at 2θ values of 20.1° and 23.6° are observed in the diffraction pattern corresponding to the d spacings of 4.41 and 3.76 Å, which corresponds to the α-crystalline form of PA6. The peak at 20.1° corresponds to plane (200) and the one at 23.6° to planes (002) and (202), respectively. In addition, a peak at 21.5° was observed, showing the presence of metastable γ-form of PA6. This peak corresponds to the (001) plane. The WAXD pattern indicated the presence of both α and γ crystalline forms of PA6 in all the blends of PA6/ABS in which the d spacings remain unaltered.

TABLE III
Overview of the Parameters Calculated from SAXS Measurements in PA6/ABS Blends and for 80/20 PA6/ABS Blends with or without SMA-modified MWNT

Code	L_w (Å)	L_c (Å)	L_a (Å)
PA6/ABS blends			
PA6	94.4	32.8	61.6
N80A20	90.0	38.7	51.3
N65A35	96.3	32.5	64.0
N60A40	96.3	27	69.2
N55A45	94.5	26.2	68.2
N50A50	93.5	23.7	69.7
80/20 PA6/ABS			
N80A20S2	93.6	36.5	57.1
N80A20M1	94.0	34.0	60.0
N80A20M2	96.5	37.0	59.5
N80A20M5	96.7	36.7	60.0

SAXS analysis

The Lorentz corrected scattering profiles (Iq^2 versus q curve) of pure PA6 together with its blends obtained at room temperature are shown in Figure 12, where I is the intensity and q is the scattering vector ($=2\pi/d$), the maxima of the peak corresponds to the long period (Lw) obeying the relationship $Lw = 2\pi/q$. Figure 12(a) compares the Iq^2 versus q plots for neat PA6 and blends of PA6/ABS. The plot for PA6 shows one peak as expected. The L_w, crystalline lamellae thickness ($L_c = X_c \times L_w$, where X_c is the degree of crystallinity obtained from the DSC scans) and amorphous interlayer thickness ($L_a = L_w - L_c$) of PA6 and its blends were calculated from the Lorentz corrected Iq^2 versus q scattering profile and are reported in Table III. In these blends, L_c is found to decrease but L_a increases with increase in ABS content (co-continuous region). It is believed that decrease in L_c is expected to give rise to thinner and less perfect crystalline lamellae resulting in a lower degree of crystallinity. The slight increase in L_a may be due to progressive broadening of the transition layer between crystalline lamellae and amorphous layer as a result of the formation of less perfect crystalline structures. These observations are in accordance with the DSC results where a decreasing trend in the degree of crystallinity was observed with increase in the ABS content. It is one of the expectations that the thinner and less perfect crystallites originate when the mobility of the polymer chains is restricted. From the flow curves [Fig. 1(a)] one can clearly observe an increase in the melt viscosity with increase in the ABS content in the blend. Thus, delayed crystallization along with an increase in the melt viscosity in the blends resulted in thin and less perfect crystallites.

Further, a unique observation is found from these scattering profiles; several scattering maxima at higher q regions ($1.0 < q < 1.4$; $1.4 < q < 1.6$) are observed for the blends, which are of co-continuous type. This is attributed to the presence of multiple lamellae stacking of different crystals of PA6 in the cocontinuous compositions. It is evident that melt viscosity of ABS might be playing a vital role during the PA6 solidification process, which can also be observed from the delayed crystallization behavior of PA6 from the DSC results. The multiple lamellae stacking of PA6 phase is also observed in 20/80 PA6/ABS blends where fractionated crystallization of PA6 is found to occur.[41]

Figure 12(b) compares the Iq^2 versus q plots for 50/50 blends of PA6/ABS with or without the presence of SMA modified by MWNT. Because of progressive broadening in the Iq^2 versus q scattering profile in case of 50/50 PA6/ABS blends, it was not possible to determine the SAXS parameters from these plots. Interestingly, the second scattering maxima is broadened either in presence of SMA or SMA modified by MWNT, which may be due to significant changes in the co-continuous morphology in

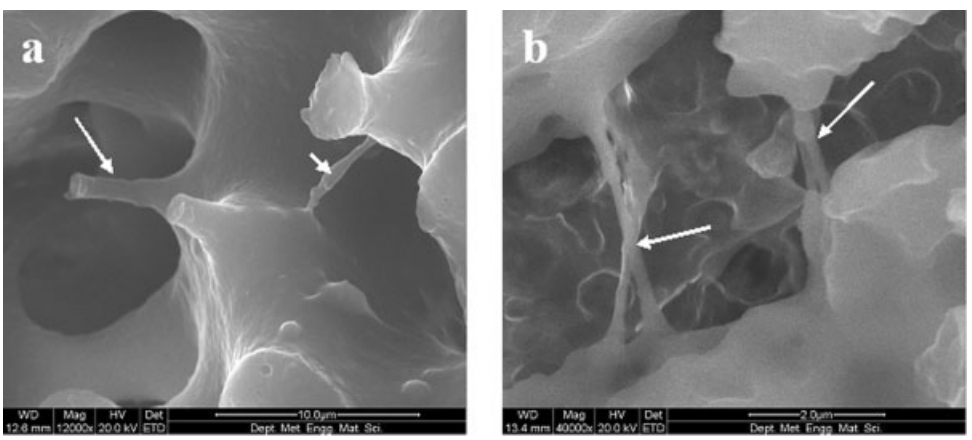

Figure 8 SEM micrographs of cryofractured and selectively etched by THF showing encapsulation of MWNT by SMA copolymer in; (a) N50A50M1; (b) N80A20M1.

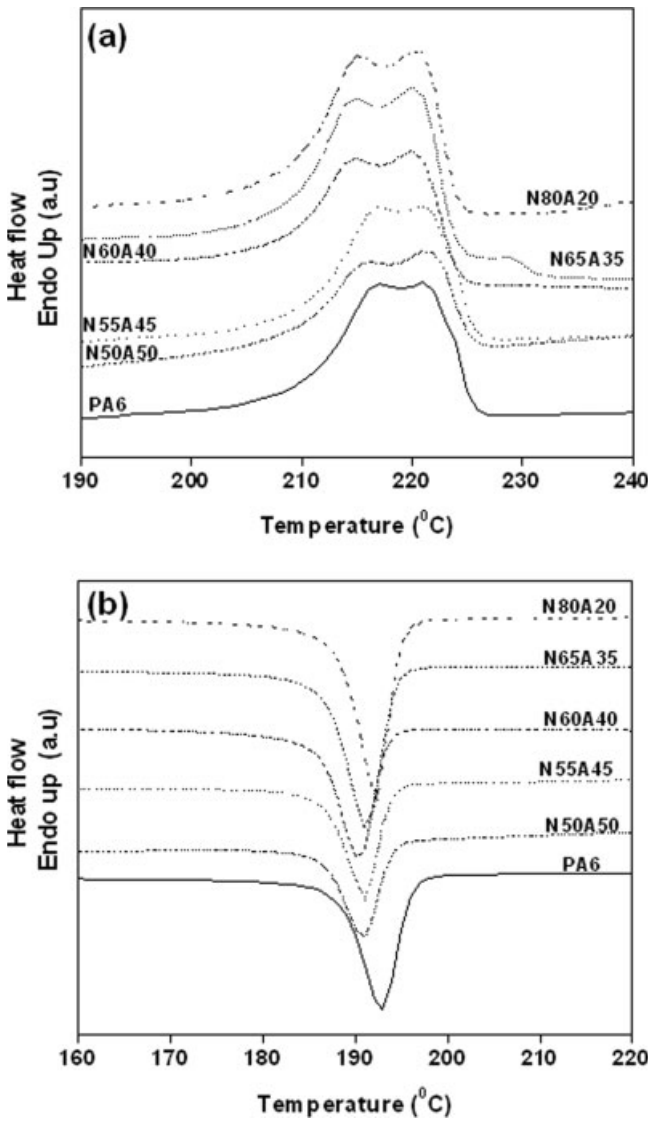

Figure 9 DSC; (a) heating; (b) cooling scans of PA6 and blends of PA6/ABS.

presence of reactive compatibilizer. Figure 12(c) compares the Iq^2 versus q plots for 80/20 blends of PA6/ABS with or without the presence of SMA modified by MWNT. It is seen from Table III that L_w and L_a increases but L_c decreases on incorporation of 2 wt % SMA as compared with neat 80/20 PA6/ABS blends indicating the miscibility in the amorphous phases in presence of the compatibilizer and significant changes in the crystalline morphology. On incorporation of SMA modified by MWNT a consistent increase in L_w is observed with increasing SMA modified by MWNT content. On the other hand the effectiveness of the compatibilizer is well evident from the significant increase in the L_a values in the compatibilized blends as compared with neat 80/20 PA6/ABS blends suggesting enhanced miscibility in presence of the compatibilizer. These observations are also consistent with both DSC and morphological analysis.

CONCLUSIONS

Polyamide6 (PA6)/acrylonitrile butadiene styrene (ABS) blends were prepared by melt-mixing where the ABS content was varied from 20 to 50 wt %. SEM analysis revealed that 80/20 PA6/ABS blends exhibit matrix-dispersed droplet morphology whereas, PA6/ABS blends containing 35–50 wt % ABS showed cocontinuous morphology. Obtained from selective extraction of ABS using THF the continuity of the ABS phase also indicated the cocontinuous structure for PA6/ABS blends beyond 20 wt % ABS content. It is found that reactive compatibilization can be assisted by modification of the compatibilizer with MWNT. A refinement in morphology was found on addition of 2 wt % styrene maleic an-

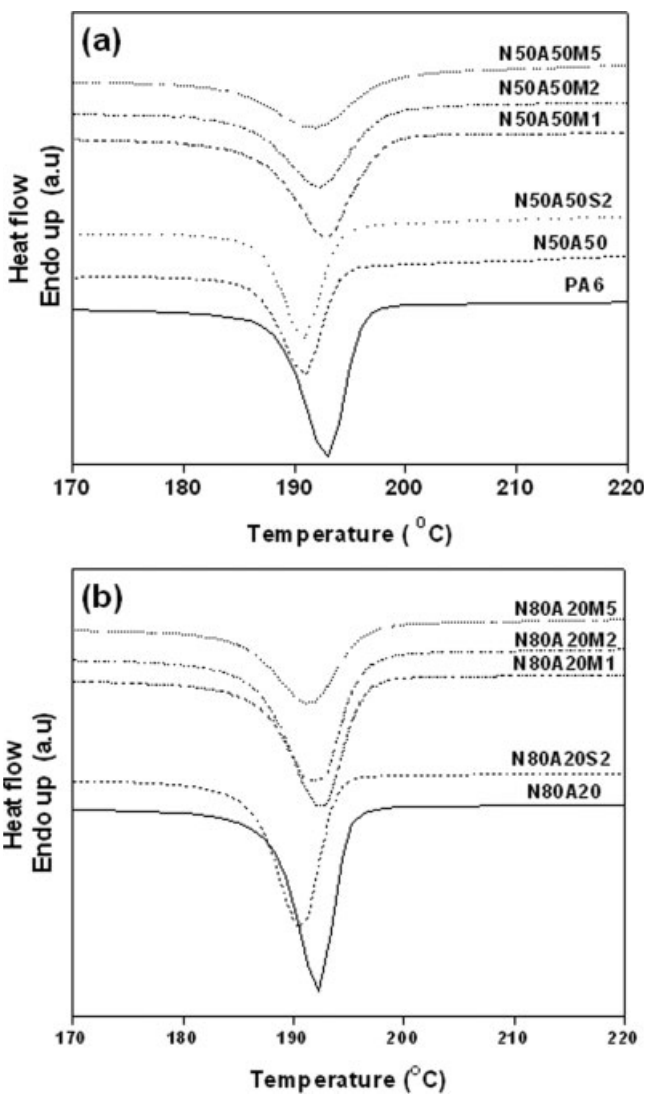

Figure 10 DSC cooling scans of (a) 50/50 PA6/ABS blends with or without SMA modified by MWNT; (b) 80/20 PA6/ABS blends with or without SMA modified by MWNT.

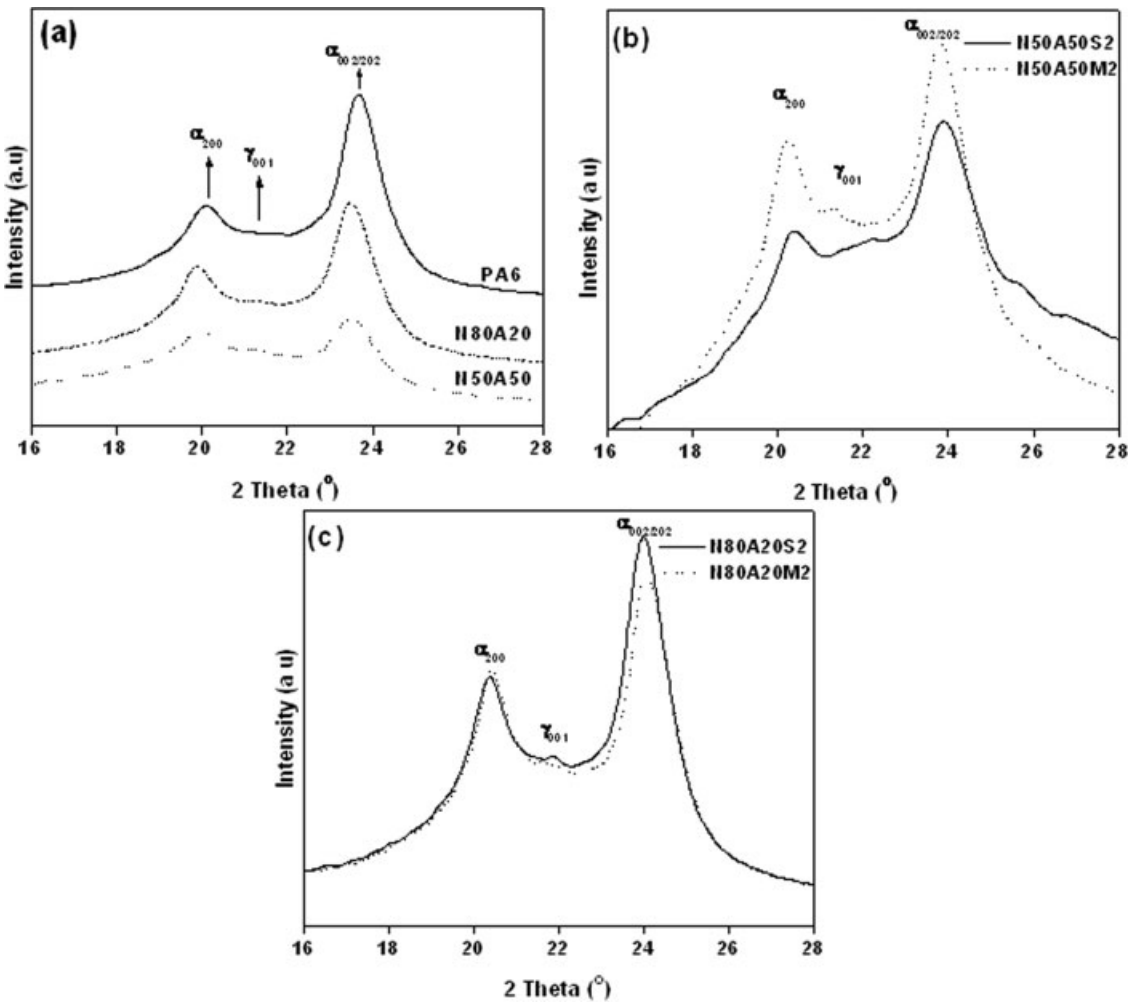

Figure 11 Wide angle X-ray diffraction patterns of (a) neat PA6 and PA6/ABS blends; (b) 50/50 PA6/ABS blends with or without SMA modified by MWNT; (c) 80/20 PA6/ABS blends with or without SMA modified by MWNT.

hydride (SMA) modified by MWNT (0.1 wt % of MWNT and 1.9 wt % of SMA) as compared with addition of 2 wt % SMA in matrix-dispersed blends (80/20) as well as in cocontinuous blends (50/50) which is presumably due to modified interphase rheology in presence of MWNT in the SMA phase. In addition, MWNT located at the interphase because of its dispersion within the reactive compatibilizer lead to a stabilization of the interphase and prevents coalescence via sterical hindrance which further contribute to the formation of smaller sized and more stable morphological features. Crystallization studies indicate delayed crystallization behavior of PA6 (manifested in lowering in T_c) in the PA6/ABS blends particularly in the co-continuous region. SAXS analysis revealed the formation of thinner and less perfect crystallites of PA6 phase in the PA6/ABS blends, which showed cocontinuous morphology. SAXS analysis further revealed a unique observation of multiple scattering maxima at higher q region in the Lorentz corrected SAXS pattern, which is attributed to the formation of multiple lamellae stacking.

Thus, it can be concluded that the use of a reactive compatibilizer (SMA modified by MWNT) in the PA6/ABS blends stabilizes the co-continuous morphology where the MWNT located at the interphase alters the rheology of the interphase and stabilize the morphology by inhibiting coalescence.

We acknowledge Microcompounder Central facility at IIT Bombay, DST-FIST sponsored SAXS facility in the Chemical Engineering Department at IIT Bombay. We are grateful to Prof. Anil Kumar (Department of Chemistry, IIT Bombay) for providing DSC facility and to Dr. Vivek Pancholi (OIM-SEM National Facility, IIT Bombay) for assistance in SEM investigations. One of the authors (ARB) thank Leibniz Institute of Polymer Research Dresden, Germany for providing ARES rheometer facility.

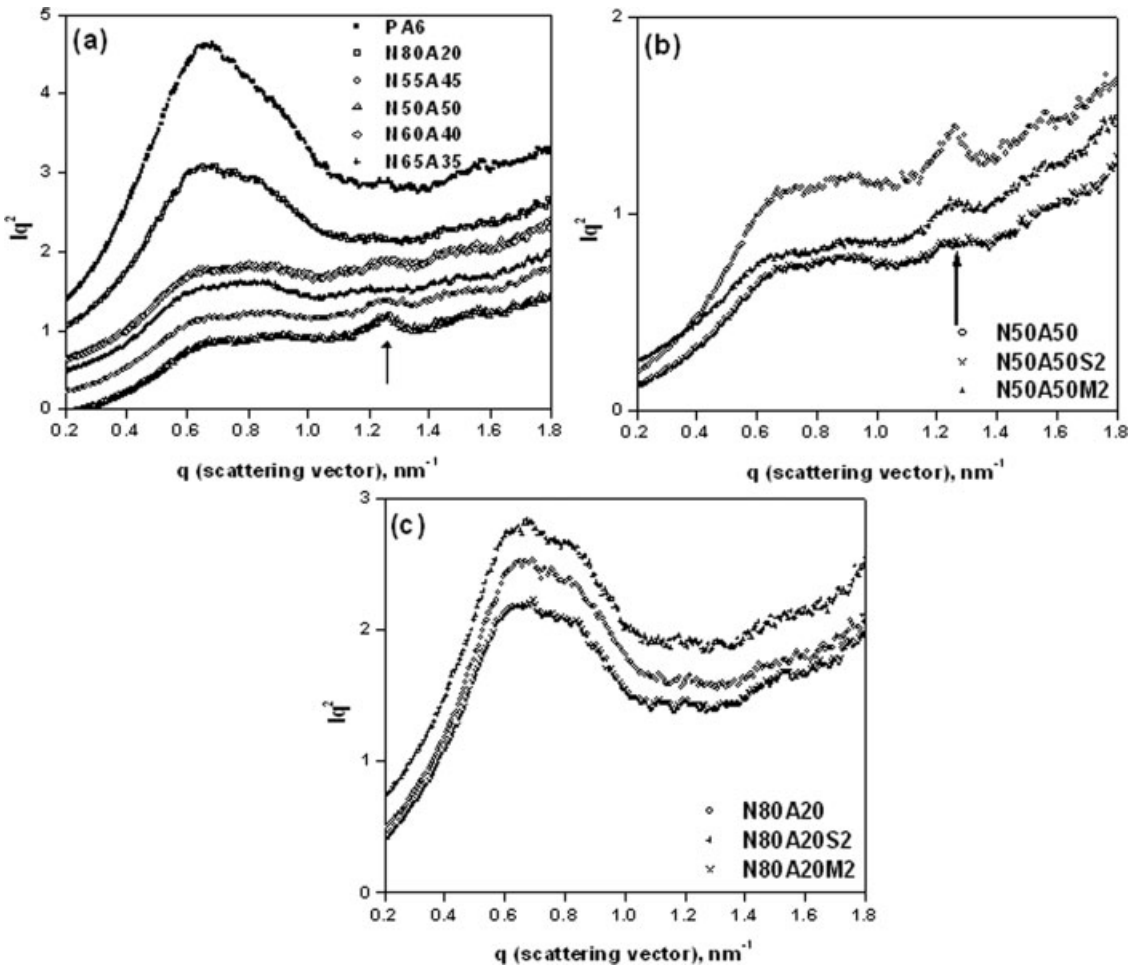

Figure 12 Lorentz corrected SAXS plots of Iq^2 versus q of (a) neat blends; (b) 50/50 PA6/ABS blends with or without SMA modified by MWNT; (c) 80/20 PA6/ABS blends with or without SMA modified by MWNT where, I is the intensity and q is the scattering vector.

References

1. Paul, D. R.; Newman, S. Polymer Blends; Academic Press: New York, 1978.
2. Utracki, L. A. Polymer Alloys and Blends; Hanser Publications: Munich, 1989.
3. Chen, C. C.; White, J. L. Polym Eng Sci 1993, 33, 923.
4. Min, K.; White, J. L.; Fellers, J. F. Polym Eng Sci 1984, 24, 1327.
5. Wu, S. Polymer Interface and Adhesion; Marcel Dekker: New York, 1982.
6. Sundararaj, U.; Macosko, C. W. Macromolecules 1995, 28, 2647.
7. Majumdar, B.; Keskkula, H.; Paul, D. R. Polymer 1994, 35, 1399.
8. Koning, C.; Duin, M. V.; Pagnoulle, C.; Jerome, R. Prog Polym Sci 1998, 23, 707.
9. Utracki, L. A. J Rheol 1991, 35, 1615.
10. Cheung, Y. W.; Stein, R. S.; Wignall, G. D.; Yang, H. E. Macromolecules 1993, 26, 5365.
11. Nadkarni, V. M.; Jog, J. P. In Handbook of Polymer Science and Engineering, Vol. 4; Marcel Dekker: New York, 1989.
12. Ikkala, O. T.; Holsti-Miettinen, R. M.; Seppälä, J. J Appl Polym Sci 1993, 49, 1165.
13. Moon, H. S.; Ryoo, B. K.; Park, J. K. J Polym Sci Part B: Polym Phys 1994, 32, 1427.
14. Oderkerk, J.; Groeninckx, G. Polymer 2002, 43, 2219.
15. Martuscelli, E.; Riva, F.; Sellitti, C.; Silvestre, C. Polymer 1985, 26, 270.
16. Bhattacharyya, A. R.; Ghosh, A. K.; Misra, A. Polymer 2001, 42, 9143.
17. Beltrame, P. L.; Castelli, A.; Canauz, M.; Seves, A. Macromol Chem Phys 1995, 196, 2751.
18. Jafari, S. H.; Pötschke, P.; Stephan, M.; Pompe, G.; Warth, H.; Alberts, H. J Appl Polym Sci 2002, 84, 2753.
19. Araujo, E. M.; Hage, E.; Carvalho, A. J. F. J Mater Sci 2004, 39, 1173.
20. Hage, E.; Ferreira, L. A. S.; Manrich, S. J Appl Polym Sci 1999, 71, 423.
21. Triacca, V. J.; Ziaee, S.; Barlow, J. W.; Keskkula, H.; Paul, D. R. Polymer 1991, 32, 1401.
22. Jang, S. P.; Kim, D. Polym Eng Sci 2000, 40, 1635.
23. Misra, A.; Sawhney, G.; Kumar, R. A. J Appl Polym Sci 1993, 50, 1179.
24. Majumdar, B.; Keskkula, H.; Paul, D. R. J Polym Sci Part B: Polym Phys 1994, 32, 2127.
25. Majumdar, B.; Keskkula, H.; Paul, D. R. Polymer 1994, 35, 3164.
26. Otterson, D. M.; Kim, B. H.; Lavengood, R. E. J Mater Sci 1991, 26, 1478.
27. Kim, B. K.; Lee, Y. M.; Jeong, H. M. Polymer 1993, 34, 2075.
28. Kudva, R. A.; Keskkula, H.; Paul, D. R. Polymer 1998, 39, 2447.

29. Aoki, Y.; Watanabe, M. Polym Eng Sci 1992, 32, 878.
30. Baer, M. (to Monsanto). U.S. Pat. 4,584,344 (1986).
31. Lavengood, R. E.; Padwa, R. A.; Harris, A. F. (to Monsanto). U.S. Pat. 4,713,415 (1987).
32. Lavengood, R. E. (to Monsanto). U.S. Pat. 4,777,211 (1988).
33. Baughman, R. H.; Zakhidov, A. A.; de Heer, W. A. Science 2002, 297, 787.
34. Bhattacharyya, A. R.; Sreekumar, T. V.; Liu, T.; Kumar, S.; Ericson, L. M.; Hauge, R. H.; Smalley, R. E. Polymer 2003, 44, 2373.
35. Valentini, L.; Biagiotti, J.; Kenny, J. M.; Santucci, S. J Appl Polym Sci 2003, 87, 708.
36. Grady, B. P.; Pompeo, F.; Shambaugh, R. L.; Resasco, D. E. J Phys Chem B 2002, 106, 5852.
37. Wu, T.-M.; Chen, E.-C. J Polym Sci Part B: Polym Phys 2006, 44, 598.
38. Ryan, K. P.; Cadek, M.; Drury, A.; Ruether, M.; Blau, W. J.; Coleman, J. N. Fullerenes, Nanotubes, Carbon Nanostruct 2005, 13, 431.
39. Pötschke, P.; Fornes, T. D.; Paul, D. R. Polymer 2002, 43, 3247.
40. Pötschke, P.; Bhattacharyya, A. R.; Janke, A. Polymer 2003, 44, 8061.
41. Bose, S.; Bhattacharyya, A. R.; Kodgire, P. V.; Misra, A. Polymer 2007, 48, 356.
42. Brandrup, J.; Immergut, E. H. Polymer Hand book, 2nd ed.; Wiley: New York, 1975.
43. Bhattacharyya, A. R.; Pötschke, P.; Häußler, L.; Fischer, D. Macromol Chem Phys 2005, 206, 2084.